Citation Information: DOI: 10.1109/JPHOTOV.2023.3308259

Comparative Evaluation of Solar Power Smoothing Techniques Considering Battery Degradation

Angelos I. Nousdilis, *Member, IEEE,* Georgios C. Kryonidis, *Member, IEEE* and Theofilos A. Papadopoulos, *Senior Member, IEEE*

***Abstract*—The intermittent and volatile nature of renewable energy sources (RESs) has introduced new technical challenges that affect the secure and reliable grid operation. These challenges can be tackled at the RES level by reducing power fluctuations with the use of power smoothing (PS) techniques. Several PS methods have been proposed in the literature to smooth RES output exploiting battery energy storage systems (BESSs). However, a comprehensive comparative evaluation of PS methods is missing. Moreover, the effect of the long-term PS operation on the BESS life is usually ignored in such analyses. This paper proposes a methodology for the systematic evaluation of well-established PS techniques, comparing their effectiveness on the PS of photovoltaics output based on various signal metrics. Additionally, an accurate aging model for lithium-ion batteries is employed to investigate the impact of PS on the BESS lifetime, highlighting the main parameters that influence capacity degradation.**

***Index Terms*—Battery energy storage systems, battery degradation, photovoltaics, power smoothing.**

I. Introduction

RENEWABLE energy sources (RESs) constitute the main drive towards the green transformation of the electrical grid. However, this transformation brings new challenges regarding the short-term and dynamic grid operation that are mainly caused by the intermittent and volatile nature of RESs [1]. This problem will deteriorate in the future due to the continuous increase of RES penetration that is primarily driven by the goal for a climate neutral European Union in 2050 [2].

According to literature, the intermittency and volatility problems can be solved either at grid or RES level. In the former case, the network operating conditions are adjusted by employing coordinated control schemes to compensate the impact of the stochastic RES output on the secure grid operation. Specifically, in [3], the well-established conservation voltage reduction method is used to smooth the power fluctuations at the point of the interconnection of the distribution with the upstream grid by actively controlling loads. A similar approach is adopted in [4] where an optimization-based demand response method is employed to mitigate power and voltage fluctuations at the distribution grid level. However, system level solutions require high investments from distribution system operators (DSOs) in control and monitoring equipment. Moreover, power quality issues may occur, e.g., voltage violations, overloading of network equipment, etc., since most of the network constraints are not considered in their implementation.

The above-mentioned issues can be efficiently addressed by reducing power fluctuations at RES level [5]. The power smoothing (PS) methods proposed in the literature can be categorized into two groups based on the use of energy storage systems (ESSs) [6]. In the first group, RESs are forced to operate at a set-point below the maximum power point (MPP). By adjusting this set-point, the RES output power can be controlled and smoothed against MPP. In particular, in [7], a virtual low-pass filter is applied to smooth the output wind power. Additionally, the authors in [8] propose a hierarchical structure to smooth the output power of a wind turbine by controlling the dc-link voltage, rotor speed, and blade pitch angle. However, all these solutions are environmentally costly, since operating below MPP leads to significant loss of green energy.

In the second group, ESSs are employed to cover the mismatch between the output power of the RES MPP, e.g., photovoltaic, and the smoothed power delivered to the grid. The most-well established ESS-based solutions proposed in the literature can be classified into the following [9]: (a) filtering algorithms (FAs) and (b) ramp-rate limitation (RRL) control schemes. In FAs, the ESS absorbs the high frequency power components of the primary energy source operating at MPP. The power components can be determined by using one of the following filtering techniques: high-pass filter [10], moving-average (MA) algorithm [11], low-pass filter (LPF) [12], Savitzky-Golay (SG) filter [13], Kalman filter (KF) [14], and wavelet analysis [15]. In RRL control schemes, the ESS is used to saturate the RES output power in cases the ramp-rate of the primary energy source exceeds a predefined limit [16]. Another variant of the RRL method is proposed in [17] where the RRL is activated only when the injected power to the grid exceeds a predefined limit. The combined operation of FA and RRL has been investigated in [18]. In particular, FA is used to alleviate fast power fluctuations, while RRL is employed to perform PS in the long-term. An alternative approach includes the use of fuzzy techniques for PS, presenting, however, a limited performance against RRL [19].

The research work was supported by the Hellenic Foundation for Research and Innovation (H.F.R.I.) under the "First Call for H.F.R.I. Research Projects to support Faculty members and Researchers and the procurement of high-cost research equipment grant" (Project Number: HFRI-FM17-229).

A. I. Nousdilis is with the Department of Electrical and Computer Engineering, University of Western Macedonia, Kozani, 50100, Greece, e-mail: a.nousdilis@uowm.gr

G. C. Kryonidis is with the School of Electrical and Computer Engineering, Aristotle University of Thessaloniki, Thessaloniki, 54124, Greece, e-mail: kryonidi@ece.auth.gr

T. A. Papadopoulos is with the Department of Electrical and Computer Engineering, Democritus University of Thrace, Xanthi, 67100, Greece, e-mail: thpapad@ee.duth.gr

Enhanced versions of the above solutions have been proposed in [20]–[22] by including the technical constraints of the ESSs, e.g., state-of-charge (SoC) limits, during PS operations. Specifically, an adaptive cutoff frequency of the high-pass filter is proposed in [20] to ensure SoC sharing among ESSs in a distribution network. Furthermore, in [21], short-term forecasts are employed to avoid SoC limit violations. In [22], a feedback control scheme is integrated to the RRL algorithm to actively control the ESS SoC within the permissible limits.

According to the above analysis, it can be derived that most of the works focus on the implementation of PS techniques without thoroughly evaluating their performance against the current state-of-the-art solutions. An initial attempt has been made in [23] by comparing several PS techniques. Nevertheless, in this analysis, no metrics have been proposed to deeply investigate the performance of the examined PS techniques and no actions were taken to ensure a common basis for the comparisons. Additionally, all the afore-mentioned control schemes ignore the effect that the adopted PS technique may have on the long-term performance of the ESS. Towards this objective, the authors in [24] have proposed a sophisticated method based on the KF to smooth the RES output power, including also the state-of-health of the ESS. However, a detailed, dynamic ESS model is used, which is not applicable for the long-term evaluation of ESS capacity degradation.

This paper attempts to fill these gaps by presenting a systematic comparative assessment of the most well-established PS techniques. Building on the previous work of [25], additional PS techniques are investigated and new metrics are proposed to evaluate their performance. To ensure a fair comparison, the PS techniques performance is assessed on a common basis. A lithium-ion battery aging model is also employed to evaluate the effect of each PS technique on the ESS capacity degradation and a sensitivity analysis is performed to identify the main parameters that influence the ESS lifetime expectancy.

II. Performance Assessment Methodology

In this paper, a new methodology is proposed for the assessment of PS techniques performance. The battery ESS (BESS) daily operation is simulated based on the specific control of each PS method, and two main outputs are exported: the smoothed PV power and the BESS SoC profile. The first is used to compare the effectiveness of the PS methods based on specific metrics, and the latter to evaluate the long-term influence of each PS technique on the BESS lifetime. To ensure a common comparative basis, all examined PS techniques (i) are modified by including a feedback control loop to recover SoC back to its reference value, and (ii) are adjusted to achieve a common ramp-rate limitation. Apart from RRL, several well-established FAs are also investigated, namely LPF, MA, SG, KF, and wavelet analysis [25].

A. Power Smoothing Techniques Under Study

The LPF is the basis for most smoothing methods. LPF tends to retain the low frequency information up to a selected cutoff frequency within the signal by reducing the high frequency components. In the present analysis, the discrete-time realization of the first-order infinite impulse response LPF is considered [25].

An alternative FA is the MA filter. MA is a simple LPF commonly used with time series data to smooth out short-term fluctuations and stress out longer-term trends or cycles. In particular, it creates series of averages of different subsets of the full data set and smooths the data by replacing each point with the average of the neighboring data points within the span. Due to its simple structure and low complexity it is the most widely used PS algorithm [25].

Closely related to the MA filter is the SG algorithm. In this design, successive sub-sets of adjacent data points are fitted by using a low-degree polynomial in a linear least-squares sense [13].

Wavelet analysis is widely used for feature detection, noise removal, and other signal processing applications. A sampled signal is decomposed on the basis of the discrete wavelet transform (DWT) into low-frequency and high-frequency components. Particularly, the wavelet function is used as the low-pass filter and its dual as the high-pass filter. The process is iterated and successive low-frequency components are derived up to a specific resolution level. Effectively, wavelet analysis is a band-pass filter with a scaling factor of powers of two in the time domain; thus, it halves the bandwidth at every subsequent level of the DWT. There are several wavelet basis functions families with one of the most known being the Daubechies [26].

The KF is a real-time recursive process [14]. It has been used into several applications, one of the most important being to filter out noisy time series data. The aim is to minimize the error between the actual noiseless and the corrected value calculated by applying probabilistic estimation. Since data are processed recursively, more accurate estimates are obtained compared to traditional FA. Moreover, the fast processing enables KF for online applications.

TABLE I
Key Design Parameters of FA

Method	Parameter
LPF	time constant (cutoff frequency)
MA	window length (model order)
SG	window length, polynomial order
DWT	window length, wavelet basis function
KF	covariance matrix

The key design parameters of FA are summarized in Table I. It can be seen that the data window size is important for most algorithms. In the case of online applications, the window size includes present as well as historical data. Nevertheless, the use of historical data always results into the so called “memory effect” that causes PV output to differ significantly from the present value of the fluctuating power [6]. A solution to the memory effect is to directly control ramp-rate of the RES output power by means of RRL algorithms [6], [16]. In such a case, the power mismatch between the primary energy and the RES output is absorbed/provided by the BESS.

B. Battery SoC Recovery Mechanism

To ensure the BESS availability for the PS operation, a battery SoC recovery mechanism is adopted. This mechanism is implemented through the linear feedback loop of Fig. 1 [22] and aims to recover the battery energy content to a predefined reference level (E_{bat}^{ref}) at the end of the day. It should be noted that, E_{bat}^{ref} can be also expressed as a percentage of the battery nominal capacity (E_{bat}^{nom}) as follows:

$$SoC_{ref} = E_{bat}^{ref} / E_{bat}^{nom} \tag{1}$$

where SoC_{ref} is the target SoC value set by the recovery mechanism.

Considering a given time instant t, the power calculated from the feedback loop (P_{fb}^{t}) is subtracted from the PV output power (P_{mpp}^{t}) and the resulted power is used as input to the PS control block. The output of this block is the smoothed PV power (P_{sm}^{t}) that is used to calculate the required BESS charging/discharging power (P_{bat}^{t}) according to (2). Eventually, the integral of P_{bat}^{t} is used to estimate the new energy content of the BESS at t (E_{bat}^{t}), taking into consideration the charging and discharging efficiency of the BESS, η_{ch} and η_{dch}, respectively. P_{fb}^{t} is defined by (3) with k being the proportional gain that regulates the convergence speed of the SoC recovery feedback loop.

$$P_{bat}^{t} = P_{mpp}^{t} - P_{sm}^{t} \tag{2}$$

$$P_{fb}^{t} = k(E_{bat}^{ref} - E_{bat}^{t}) \tag{3}$$

C. Battery Degradation Model

The lithium-ion battery degradation model of [27] is adopted for the evaluation of the battery capacity loss. First, the BESS SoC profile for time period T is imported in the model. Since PS may not result in full charging-discharging cycles, the BESS SoC profile is analyzed exploiting the rainflow algorithm [28] to obtain all equivalent full and half cycles within T. The battery cells degradation at the end of analysis period T is a result of the calendar and the cyclic aging mechanisms. The calendar aging is represented by degradation factor f_{cal} and the cyclic aging by factor f_{cyc}^{k} for each k cycle.f_{cal} is a function of the average cell temperature and the average SoC over the elapsed time; f_{cyc}^{k} is affected by the average SoC, the depth-of-discharge (DoD) and the average temperature of the k-th cycle. After f_{cal} and f_{cyc}^{k} are calculated, the overall degradation factor, f_d, is determined by (4), for all cycles N within T.

$$f_d = f_{cal} + \sum_{k}^{N} f_{cyc}^{k} \tag{4}$$

Finally, the BESS capacity loss (L^T) over T is derived by (5):

$$L^T = 1 - \alpha_{sei} e^{-\beta_{sei} f_d} - (1 - \alpha_{sei}) e^{-f_d}. \tag{5}$$

The first exponential term of (5) pertains to the fast aging stage occurring during the early cycles of the battery life, caused mainly by the formation of the solid electrolyte interphase (SEI) film [29]. Parameters α_{sei} and β_{sei} characterizing this early aging stage are acquired through battery aging tests. The second exponential term of (5) represents the capacity loss after the SEI film formation stage.

TABLE II
BESS CHARACTERISTICS

Capacity	5 kWh	SoC_{ref}	50%
Inverter efficiency	98%	SoC_{init}	50%
Charging/discharging efficiency	97%	SoC_{min}	10%
Rated power	5 kW	SoC_{max}	95%

D. Long-term Assessment Methodology

To evaluate the long-term performance of the PS techniques as well as their effect on BESS aging, the methodology of Fig. 2 is developed. First, the PV and load power time series for the time period of a day (d) are imported. Afterwards, the daily BESS power determined by the examined PS technique is simulated and the extracted SoC profile is used to obtain the battery capacity fade up to T using (5). Finally, the BESS capacity, $Cap(T)$, is updated using (6):

$$Cap(T) = (1 - L^T) Cap(0) \tag{6}$$

where $Cap(0)$ is the rated capacity of the battery. The described process is iterated with a daily timestep until the BESS capacity reaches the end of its life, defined here as the 80% of its rated value [30].

III. Numerical Results

A. System Under Study

To assess the performance of the PS techniques and their effect on battery lifetime, a PV-battery system is considered consisting of 5 kWp PV and a BESS with the characteristics of Table II. Specifically, in this Table SoC_{min} and SoC_{max} denote the minimum and the maximum permissible SoC values, respectively, and SoC_{init} stands for the initial SoC value at the beginning of the simulation. PV output power is calculated based on the solar irradiation measured for a sunny and a cloudy day in Thessaloniki, Greece. The daily PV power is iterated to form a year with a random distribution of sunny and cloudy days, considering that 30% of the days within the year are cloudy. It is assumed that the BESS is equipped with a ventilation system that keeps the battery cell temperature constantly at 20°C.

B. Comparative Assessment of PS Techniques Performance

To achieve a common basis for the comparisons, the SoC recovery gain is assumed as $k = 2\,\mathrm{h}^{-1}$ and the permissible PV power ramp-rate limit (RR_{lim}) is set at 4 W/s [31] for all methods. The key design parameters of the examined PS methods are adjusted accordingly, as shown in Table III, to guarantee that (7) is satisfied throughout the day, where $RR(t)$ represents the absolute value of the PV power ramp-rate.

$$RR(t) \ \leq RR_{lim}, \forall t \in d \tag{7}$$

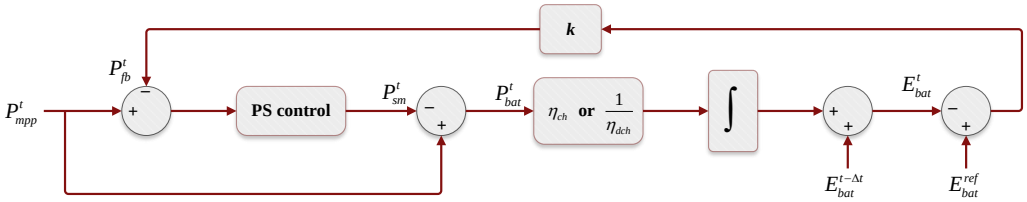

Fig. 1. Control loop for battery SoC recovery mechanism.

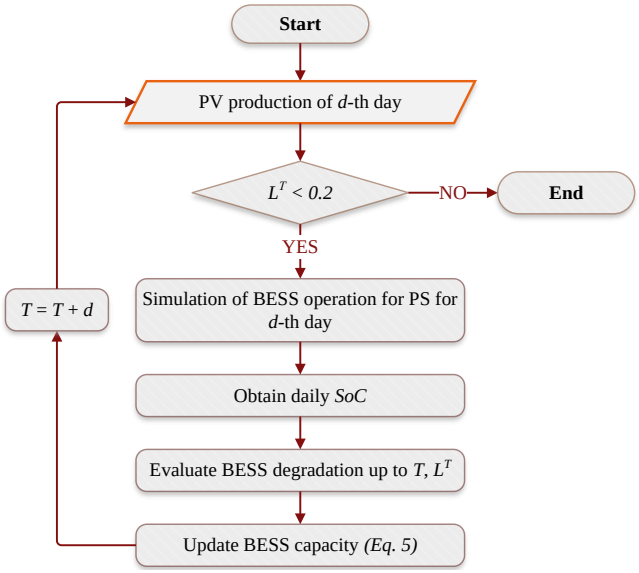

Fig. 2. Long-term BES capacity degradation assessment methodology.

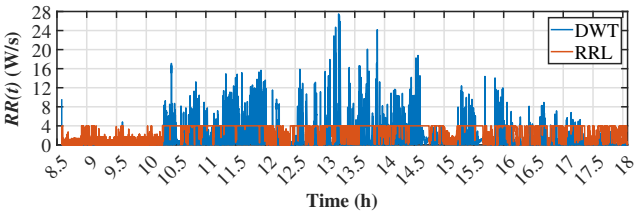

Fig. 3. $RR(t)$ throughout the PV production period after employing the PS technique based on RRL and on DWT.

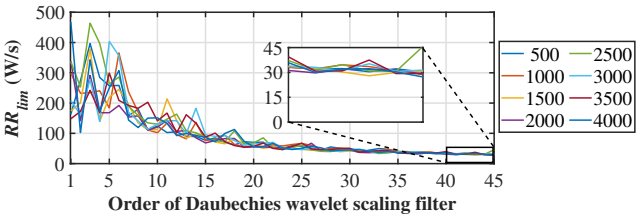

Fig. 4. RR^{max} achieved by using wavelets of the Daubechies family for various window lengths.

TABLE III
PS METHODS PARAMETERS TO ACHIEVE RR_{lim}=4 W/S.

PS method	Method parameters	
LPF	T_{lpf}=455 s	
MA	T_{ma}=125 s	
SG	T_{sg}=3400 s	1st polynomial order
DWT	T_{sg}=4000 s	Daubechies (order 45)
KF	a=0.5	b=454
RRL	RR^{max}=4 W/s	RR^{min}=4 W/s

It is worth mentioning that DWT cannot achieve the specified RR_{lim}. Indeed, as shown in Fig. 3, when the RRL method is employed, $RR(t)$ is always below the selected RR_{lim} of 4 W/s. With the DWT-based PS method, this limit is exceeded by far reaching values up to 28 W/s. To achieve the specific RR_{lim}, different Daubechies family orders (1 to 45) and window lengths (500 to 4000 s) have been tested. However, all of the key design parameter combinations led to RR_{lim} violation. The lowest RR_{lim} that is achieved throughout the PV production time period by each combination is shown in Fig. 4, indicating that wavelets are unable to achieve $RR(t)$ lower than 28 W/s. For this reason, this method is excluded from the rest of the analysis.

The MPP output power and the smoothed power after applying each PS technique are indicatively plotted for a cloudy day in Fig. 5. The resulted power curves present different level of smoothness depending on the applied PS technique. Smoother power curves are resulted by applying MA, KF, LPF, and SG, compared to the RRL method. Moreover, it can be observed that KF and LPF lead to identical PS results. This is attributed to the structure of the KF, that reduces to a first-order LPF in single signal analysis [14]. It is also shown that the MA method fails to achieve PS throughout the day for $k = 2\ \text{h}^{-1}$. This is because the SoC reaches the low limit at the period 14:50–15:40 (see Fig. 6), thus restricting further BESS discharging. For this reason, $k = 4\ \text{h}^{-1}$ is also examined for the MA method. In this case, PS is successfully achieved, i.e., $RR(t) < RR_{lim}$ throughout the day, and thus $k = 4\ \text{h}^{-1}$ is adopted for MA for the remaining of the paper.

The mitigation of $RR(t)$ for all PS methods is statistically analyzed by means of blox plots in Fig. 7 for a cloudy day. Considering the RRL method, the median $RR(t)$ is 4 W/s and the resulted box plot is wider than the rest methods. This happens because the limitation is activated only when $RR(t) > RR_{lim}$ and thus all $RR(t)$ values below RR_{lim} are permitted. In contrary, all FA methods present a relatively lower median, approximately 0.4 W/s and narrower box plots. This means that $RR(t)$ is unnecessarily reduced even in cases RR_{lim} is not exceeded, resulting into smoother $P_{sm}(t)$ throughout the day (see Fig. 5).

In addition, the energy utilization of the BESS in terms of the total energy charged and discharged within the daily operation is presented in Table IV. It can be seen that FA methods lead to excessive energy utilization to achieve this smoother $P_{sm}(t)$, compared to the RRL method. Note that, a high energy amount indicates larger depth of discharge, which in turn affects negatively the battery life expectancy. From all FA methods, MA achieves the strictest ramp-rate limitation, presenting a median $RR(t)$ of 0.28 W/s (see Fig. 7) and

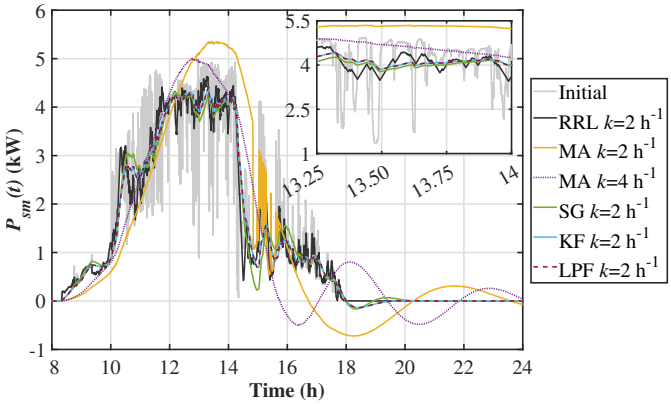

Fig. 5. Initial and smoothed PV output for various PS methods.

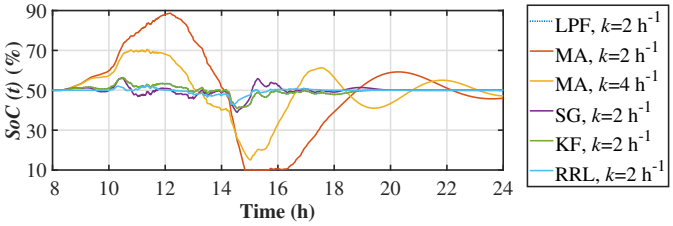

Fig. 6. Battery SoC of a cloudy day for the examined PS methods.

consequently the highest BESS energy utilization.

To systematically investigate the performance of the PS techniques, three well-established signal analysis metrics are adopted. The mean squared error (MSE) and the root mean square error ($RMSE$), given in (8) and (9), respectively, quantify the deviation of the smoothed PV power time series from the MPP output time series, throughout a certain time period consisting of N samples. A high value of these metrics demonstrates a smoother PV output power curve. As shown in Table V, MA achieves the highest value of these metrics, since it provides a smoother power profile than other methods. This is also substantiated by the results of Fig. 5 and by the median $RR(t)$ when using MA, which is the lowest among other methods. On the contrary, RRL provides the lowest MSE and $RMSE$, meaning that the deviation between the smoothed power and the MPP output profile is lower than in all other methods. This is expected due to the more relaxed $RR(t)$ limitation. Note that a higher value in the metrics results in higher energy utilization of the BESS.

$$MSE = \frac{1}{N}\sum_{t_i=1}^{N}\left(P_{sm}^{t_i} - P_{mpp}^{t_i}\right)^2, \forall t_i \in N \tag{8}$$

$$RMSE = \sqrt{MSE} \tag{9}$$

The third metric is the sample entropy ($SampEn$) [32]. It is a statistical index depicting the randomness of a series of data and is used to quantify the smoothness of the PV power time series after PS application. Contrary to MSE and $RMSE$, $SampEn$ does not compare the smoothed power to the MPP output power profile, but evaluates the randomness of the data within a single time series for a given time period.

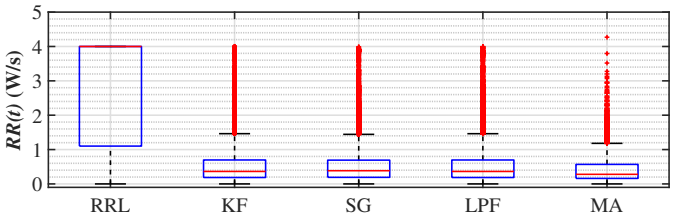

Fig. 7. Absolute value of ramp-rates for a cloudy day.

TABLE IV
DAILY TOTAL (CHARGED AND DISCHARGED) BESS ENERGY.

	RRL	LPF	MA	SG	KF
Energy (kWh)	3.12	4.32	9.25	4.85	4.32
Change vs. RRL	-	+39%	+197%	+56%	+39%

Specifically, the $SampEn$ values in Table V refer to the 24 h P_{sm}^{t} time series. A lower value of $SampEn$ pertains to a smoother power profile. As expected, MA presents the lowest and RRL the highest $SampEn$ among other methods. Note that, higher $SampEn$ values are characterized by lower BESS utilization levels.

C. Battery Lifetime Analysis

The impact of the PS methods on the battery lifetime is derived by applying the long-term assessment methodology of Fig. 2. Based on the results of Fig. 8, it is shown that the RRL achieves the longer battery lifetime compared to FAs. This is mainly attributed to the lower daily energy usage from the battery, and thus the fewer and narrower battery cycles needed to achieve PS, as shown in Fig. 6. Among all techniques, MA results in higher battery degradation since it reaches a larger DoD, as illustrated in Fig. 6, and uses the largest daily amount of battery energy. It is remarkable that, as for the same battery capacity, a higher SoC_{ref} leads to faster battery degradation, since it increases the average SoC, which in turn results into higher calendar and cyclic degradation factors. Moreover, for the same SoC_{ref}, a higher battery capacity leads to longer lifetime as observed in Fig. 8 for the case of $SoC_{ref} = 50\%$. This is explained by the fact that lower BESS capacities lead to higher DoD, considering the same battery energy required for PS.

D. Impact of Reference SoC Level on Battery Lifetime

A sensitivity analysis is performed to evaluate the impact of SoC_{ref} on the BESS degradation, which eventually influences the average SoC level of the battery charging-discharging cycles and the average SoC throughout the BESS lifetime. These two parameters play an important role in the resulted cyclic and calendar aging of the BESS, respectively. Investigating the case of a 5 kWh BESS operating under the RRL technique, SoC_{ref} is varied in the range of 20% to 80% with a 2.5% step. The BESS lifetime is strongly influenced by SoC_{ref} as demonstrated in Fig. 9. A low SoC_{ref}, e.g., 20%, prolongs the battery lifetime to more than 18 years. A high SoC_{ref} of 80% may cause 8 years reduction of BESS lifetime. It is

TABLE V
PS PERFORMANCE METRICS FOR A CLOUDY DAY.

	RRL	LPF	MA	SG	KF
MSE	0.330	0.457	1.012	0.524	0.456
$RMSE$	0.574	0.676	1.006	0.724	0.676
$SampEn$* (x10^{-4})	45.1	7.79	5.27	9.47	7.81

* A value of m=1 and r=0.2 are used for $SampEn$ metric [32]. It is also noted that P^t_{mpp} timeseries presents a $SampEn$ value of $293 \cdot 10^{-4}$.

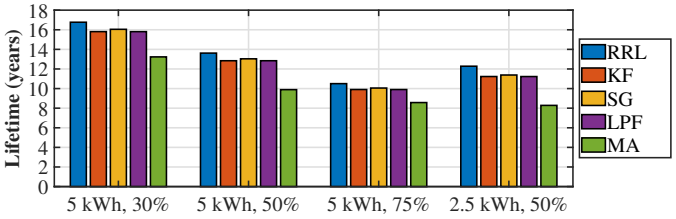

Fig. 8. Impact of the selected PS technique, the installed BESS capacity, and the selected SoC_{ref} (30%, 50%, and 75%), on the battery lifetime.

worth noting that the relation between the battery lifetime and SoC_{ref} is not linear and can be expressed by a second order polynomial.

IV. CONCLUSIONS

This paper proposes a methodology for the systematic evaluation of PS techniques, in regards with (i) their performance in smoothing the PV output power and (ii) their effect on the battery lifetime expectancy. The PS methods based on FAs result in a smoother power profile compared to the RRL technique, limiting the ramp-rate even when the selected boundary is not exceeded; thus leading to excessive BESS operation. The highest BESS energy utilization is observed when the MA-based PS technique is used. It is also noticeable that the PS method based on wavelets is unable to achieve the desired ramp-rate limitation. The level of smoothness of the PV output power achieved by each PS method is quantified through signal analysis metrics. Moreover, it is demonstrated that the average SoC level and the DoD play an important role in the battery capacity loss. These two parameters are affected by the PS technique, the selected reference SoC value, and the installed battery capacity. Based on the results of this study, when lithium-ion batteries are employed for PS, the RRL technique alongside with a low reference SoC value are suggested to prolong the life of battery.

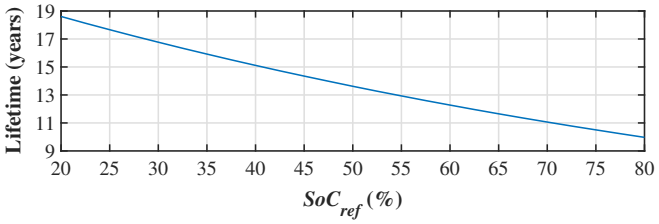

Fig. 9. Impact of SoC_{ref} on the battery lifetime for the RRL PS method.

REFERENCES

[1] V. B. Venkateswaran, D. K. Saini, and M. Sharma, "Approaches for optimal planning of energy storage units in distribution network and their impacts on system resiliency," *CSEE J. Power Energy Syst.*, vol. 6, no. 4, pp. 816–833, 2020.

[2] *A European strategic long-term vision for a prosperous, modern, competitive and climate neutral economy*, European Commission, COM 773 final, Brussels, Belgium, 2018, pp. 1–25.

[3] J. Xu, B. Xie, S. Liao, D. Ke, Y. Sun, X. Jiang, and J. Yu, "CVR based real-time power fluctuation smoothing control for distribution systems with high penetration of PV and experimental demonstration," *IEEE Trans. Smart Grid*, pp. 1–1, 2022.

[4] J. Xu, H. Fu, S. Liao, B. Xie, D. Ke, Y. Sun, X. Li, and X. Peng, "Demand-side management based on model predictive control in distribution network for smoothing distributed photovoltaic power fluctuations," *J. Modern Power Syst. Clean Energy*, pp. 1–11, 2022.

[5] G. C. Kryonidis *et al.*, "Ancillary services in active distribution networks: A review of technological trends from operational and online analysis perspective," *Renew. Sustain. Energy Rev.*, vol. 147, p. 111198, 2021.

[6] S. Sukumar, H. Mokhlis, S. Mekhilef, M. Karimi, and S. Raza, "Ramp-rate control approach based on dynamic smoothing parameter to mitigate solar PV output fluctuations," *Int. J. Electr. Power & Energy Syst.*, vol. 96, pp. 296–305, 2018.

[7] K. Liao, D. Lu, M. Wang, and J. Yang, "A low-pass virtual filter for output power smoothing of wind energy conversion systems," *IEEE Trans. Ind. Electron.*, vol. 69, no. 12, pp. 12 874–12 885, 2022.

[8] X. Lyu, J. Zhao, Y. Jia, Z. Xu, and K. Po Wong, "Coordinated control strategies of pmsg-based wind turbine for smoothing power fluctuations," *IEEE Trans. Power Syst.*, vol. 34, no. 1, pp. 391–401, 2019.

[9] X. Lyu, Y. Jia, Z. Xu, and J. Østergaard, "Mileage-responsive wind power smoothing," *IEEE Trans. Ind. Electron.*, vol. 67, no. 6, pp. 5209–5212, 2020.

[10] J. Pegueroles-Queralt, F. D. Bianchi, and O. Gomis-Bellmunt, "A power smoothing system based on supercapacitors for renewable distributed generation," *IEEE Trans. Ind. Electron.*, vol. 62, no. 1, pp. 343–350, 2015.

[11] Q. Jiang and H. Wang, "Two-time-scale coordination control for a battery energy storage system to mitigate wind power fluctuations," *IEEE Trans. Energy Convers.*, vol. 28, no. 1, pp. 52–61, 2013.

[12] N. Kakimoto, H. Satoh, S. Takayama, and K. Nakamura, "Ramp-rate control of photovoltaic generator with electric double-layer capacitor," *IEEE Trans. Energy Convers.*, vol. 24, no. 2, pp. 465–473, 2009.

[13] Y. Zhu and J. V. Milanović, "Automatic identification of power system load models based on field measurements," *IEEE Trans. Power Syst.*, vol. 33, no. 3, pp. 3162–3171, 2018.

[14] R. E. Kalman, "A new approach to linear filtering and prediction problems," *J. Basic Eng.*, vol. 82, no. 1, pp. 35–45, 1960.

[15] T. Guo, Y. Liu, J. Zhao, Y. Zhu, and J. Liu, "A dynamic wavelet-based robust wind power smoothing approach using hybrid energy storage system," *Int. J. Electr. Power & Energy Syst.*, vol. 116, p. 105579, 2020.

[16] I. de la Parra, J. Marcos, M. García, and L. Marroyo, "Control strategies to use the minimum energy storage requirement for PV power ramp-rate control," *Solar Energy*, vol. 111, pp. 332–343, 2015.

[17] V. T. Tran, M. R. Islam, D. Sutanto, and K. M. Muttaqi, "Mitigation of solar PV intermittency using ramp-rate control of energy buffer unit," *IEEE Trans. Energy Convers.*, vol. 34, no. 1, pp. 435–445, 2019.

[18] S. Patel, M. Ahmed, and S. Kamalasadan, "A novel energy storage-based net-load smoothing and shifting architecture for high amount of photovoltaics integrated power distribution system," *IEEE Trans. Ind. Appl.*, vol. 56, no. 3, pp. 3090–3099, 2020.

[19] W. C. de Carvalho, R. P. Bataglioli, R. A. Fernandes, and D. V. Coury, "Fuzzy-based approach for power smoothing of a full-converter wind turbine generator using a supercapacitor energy storage," *Elect. Power Syst. Res.*, vol. 184, p. 106287, 2020.

[20] L. Meng, T. Dragicevic, and J. M. Guerrero, "Adaptive control design for autonomous operation of multiple energy storage systems in power smoothing applications," *IEEE Trans. Ind. Electron.*, vol. 65, no. 8, pp. 6612–6624, 2018.

[21] Y. Zhou, Z. Yan, and N. Li, "A novel state of charge feedback strategy in wind power smoothing based on short-term forecast and scenario analysis," *IEEE Trans. Sustain. Energy*, vol. 8, no. 2, pp. 870–879, 2017.

[22] X. Li, D. Hui, and X. Lai, "Battery energy storage station (BESS)-based smoothing control of photovoltaic (PV) and wind power generation fluctuations," *IEEE Trans. Sustain. Energy*, vol. 4, no. 2, pp. 464–473, 2013.

[23] M. A. Syed and M. Khalid, "Moving regression filtering with battery state of charge feedback control for solar PV firming and ramp rate curtailment," *IEEE Access*, vol. 9, pp. 13 198–13 211, 2021.

[24] D. Lamsal, V. Sreeram, Y. Mishra, and D. Kumar, "Smoothing control strategy of wind and photovoltaic output power fluctuation by considering the state of health of battery energy storage system," *IET Renew. Power Gener.*, vol. 13, no. 4, pp. 578–586, 2019.

[25] G. C. Kryonidis, A. I. Nousdilis, K. D. Pippi, and T. A. Papadopoulos, "Impact of power smoothing techniques on the long-term performance of battery energy storage systems," in *2021 56th Int. Univ. Power Eng. Conf. (UPEC)*, 2021, pp. 1–6.

[26] Q. Jiang and H. Hong, "Wavelet-based capacity configuration and coordinated control of hybrid energy storage system for smoothing out wind power fluctuations," *IEEE Trans. Power Syst.*, vol. 28, no. 2, pp. 1363–1372, 2013.

[27] B. Xu, A. Oudalov, A. Ulbig, *et al.*, "Modeling of Lithium-Ion Battery Degradation for Cell Life Assessment," *IEEE Trans. Smart Grid*, vol. 9, no. 2, pp. 1131–1140, 2018.

[28] A. Nieslony, "Rainflow Counting Algorithm," *MATLAB Central File Exchange*, accessed on June 28, 2023. [Online]. Available: https://www.mathworks.com/matlabcentral/fileexchange/3026-rainflow-counting-algorithm

[29] I. Laresgoiti, S. Käbitz, M. Ecker, and D. U. Sauer, "Modeling mechanical degradation in lithium ion batteries during cycling: Solid electrolyte interphase fracture," *J. Power Sources*, vol. 300, pp. 112–122, 2015.

[30] M. Soltani, J. Ronsmans, and J. Van Mierlo, "Cycle life and calendar life model for lithium-ion capacitor technology in a wide temperature range," *J. Energy Storage*, vol. 31, p. 101659, 2020.

[31] H. Beltran, I. Tomás García, J. C. Alfonso-Gil, and E. Pérez, "Levelized cost of storage for Li-Ion batteries used in PV power plants for ramp-rate control," *IEEE Trans. Energy Convers.*, vol. 34, no. 1, pp. 554–561, 2019.

[32] A. Delgado-Bonal and A. Marshak, "Approximate entropy and sample entropy: A comprehensive tutorial," *Entropy*, vol. 21, no. 6, 2019.